THE JOURNAL OF BIOLOGICAL CHEMISTRY VOL. 281, NO. 44, pp. 33677–33683, November 3, 2006

Real-time and Single Fibril Observation of the Formation of Amyloid β Spherulitic Structures*[S]

Received for publication, June 26, 2006, and in revised form, August 24, 2006 Published, JBC Papers in Press, September 7, 2006, DOI 10.1074/jbc.M606072200

Tadato Ban[‡§1], Kenichi Morigaki[§], Hisashi Yagi[‡], Takashi Kawasaki[§], Atsuko Kobayashi[§], Shunsuke Yuba[§], Hironobu Naiki[¶], and Yuji Goto[‡2]

From the From [‡]Institute for Protein Research, Osaka University, and CREST, Japan Science and Technology Agency, Yamadaoka 3-2, Suita, Osaka 565-0871, the [§]National Institute of Advanced Industrial Science and Technology, Research Institute for Cell Engineering, Midorigaoka 1-8-31, Ikeda, Osaka 563-8577, and the [¶]Department of Pathological Sciences, Faculty of Medical Sciences, University of Fukui and CREST, Japan Science and Technology Agency, Matsuoka, Fukui 910-1193, Japan

In Alzheimer disease, amyloid β, a 39–43-residue peptide produced by cleavage from a large amyloid precursor protein, undergoes conformational change to form amyloid fibrils and deposits as senile amyloid plaques in the extracellular cerebral cortices of the brain. However, the mechanism of how the intrinsically linear amyloid fibrils form spherical senile plaques is unknown. With total internal reflection fluorescence microscopy combined with the use of thioflavin T, an amyloid-specific fluorescence dye, we succeeded in observing the formation of the senile plaque-like spherulitic structures with diameters of around 15 μm on the chemically modified quartz surface. Real-time observation at a single fibrillar level revealed that, in the absence of tight contact with the surface, the cooperative and radial growth of amyloid fibrils from the core leads to a huge spherulitic structure. The results suggest the underlying physicochemical mechanism of senile plaque formation, essential for obtaining insight into prevention of Alzheimer disease.

In Alzheimer disease, amyloid β (Aβ)[3] peptide forms amyloid fibrils that deposit in the extracellular space of the brain as senile amyloid plaques, pathological hallmarks of Alzheimer disease, and also in the walls of cerebral blood vessels (1–5). The formation of Aβ amyloid fibrils is considered to be a nucleation-dependent process in which Aβ peptides slowly associate to form a nucleus, which then grows via an extension reaction involving the sequential incorporation of Aβ peptides, producing rigid and straight morphology consisting of several layers of cross-β sheets (6, 7). This process is influenced by several factors, *i.e.* peptide concentration, pH, ionic strength, and interactions with other components (8, 9). The interactions with lipid membranes in particular have received attention because the membrane surface might be responsible for both neurotoxicity and senile plaque formation (10–12).

For several proteins including Aβ, amyloid fibrils prepared on the solid substrates such as mica or quartz produce radial assemblies (13–15). Considering that in several neurodegenerative diseases, radial and spherical aggregates of amyloid fibrils are found in tissue deposits (5, 16), surface interaction may play dominant roles in the formation of amyloid fibrils and their deposition *in vivo* (7, 17). Moreover, amyloid deposits are found in a specific tissue region, suggesting that a specific surface chemistry is involved in the fibril formation and deposition processes in general. However, the behavior of amyloid fibrils on solid surfaces is still far from clear. To obtain further insight into the mechanism of senile plaque formation and the effects of surface, direct observations are needed.

We previously developed a unique approach to monitoring fibril growth in real time at the single fibril level (18, 19), in which TIRFM was combined with the use of thioflavin T, an amyloid-specific fluorescence dye (20). With this approach, we focused on the effects of the physicochemical properties of surface on the growth of amyloid fibrils of Aβ.

EXPERIMENTAL PROCEDURES

Chemical Modification of Surfaces—Octadecyltriethoxysilane (OTS) was purchased from Shin-Etsu Chemical (Tokyo, Japan). Aminopropyltriethoxysilane (APTS) was obtained from Tokyo Kasei Kogyo (Tokyo, Japan). Polystyrenesulfonate (PSS: molecular weight (M_r) 70,000), polyacrylic acid (PAA: M_r 30,000), and polyvinylsulfonate (PVS: M_r unknown) were purchased from Sigma. Polyethyleneimine (PEI: M_r 60,000) was obtained from Nacalai tesque (Kyoto, Japan). 10-(Carbomethoxy) decyldimethylchlorosilane (CMDDS: M_r 292.92) was purchased from Gelest (Morrisville, PA).

The surface of quartz slides was modified either by adsorbing polyelectrolytes or by grafting a silane monolayer with a functional terminal group (21). In both cases, either positively or negatively charged surfaces were generated by the chemical species directly exposed to the solution (the uppermost polyelectrolyte layer or the terminal group of silane). Quartz slides were first cleaned with 0.5% (v/v) Hellmanex (Hellma, Müllheim, Germany)/water and then treated with a solution of

* This work was supported by grants from the Takeda Science Foundation and by Grant-in-Aid 40153770 from the Japanese Ministry of Education, Culture, Sports, Science and Technology on Priority Areas. The costs of publication of this article were defrayed in part by the payment of page charges. This article must therefore be hereby marked "*advertisement*" in accordance with 18 U.S.C. Section 1734 solely to indicate this fact.

[S] The on-line version of this article (available at http://www.jbc.org) contains three supplemental figures, two supplemental references, and two movies.

[1] A recipient of a Japan Society for Promotion of Science (JSPS) Post Doctoral Fellowship.

[2] To whom correspondence should be addressed. Fax: 81-6-6879-8616; E-mail: ygoto@protein.osaka-u.ac.jp.

[3] The abbreviations used are: Aβ, amyloid β; TIRFM, total internal reflection fluorescence microscopy; ThT; thioflavin T; PEI, polyethyleneimine; PVS, polyvinylsulfonate; CMDDS, 10-(Carbomethoxy)decyldimethylchlorosilane; APTS, aminopropyltriethoxysilane; PAA, polyacrylic acid; PSS, polystyrenesulfonate; OTS, octadecyltriethoxysilane.

NH_4OH (28% w/v)/H_2O_2 (30% w/v)/H_2O (0.05:1:5, v/v/v) for 15 min at 65 °C, rinsed extensively with distilled water, and finally dried in a vacuum oven at 110 °C (21). Hydrophobic substrates were prepared by the silanization of OTS (21, 22). For the silanization, quartz slides were incubated in an OTS solution (0.04% w/v in tetrahydrofuran/cyclohexane (1:20, v/v)) and subsequently annealed at 110 °C for 30 min. Positively charged surfaces were prepared by the silanization of APTS (23) or adsorption of PEI by incubating quartz in aqueous solutions of APTS (1% w/v) or PEI (0.1% w/v) (21, 24). Negatively charged surfaces were prepared either by layer-by-layer deposition of polyelectrolytes or by using a self-assembled monolayer of silanes (21, 25). The former type was created by the adsorption of PSS, PAA, or PVS onto positively charged surfaces of PEI or APTS. The other type of negatively charged surface was prepared by silanization of the substrate with CMDDS followed by hydrolysis of the ester terminal group, forming a monolayer of 10-(carboxy)decyldimethylchlorosilane.

Water contact angles were determined with a contact angle meter (Kyowa Interface Science, Saitama, Japan) at room temperature. Data were averages of the measurements of at least three spots.

Direct Observation of Amyloid Fibrils—The TIRFM system used to observe individual amyloid fibrils was developed based on an inverted microscope (IX70, Olympus, Tokyo, Japan) as described (18, 19, 26). The ThT molecule was excited at 442 nm by a helium-cadmium laser (IK5552R-F, Kimmon, Tokyo, Japan). The fluorescence image was filtered with a bandpass filter (D490/30, Omega Optical, Brattleboro, VT) and visualized using a digital steel camera (DP70, Olympus).

Aβ-(1–40) peptides were purchased from the Peptide Institute (Osaka, Japan). The purity was >95% according to the elution pattern of high performance liquid chromatography. Aβ-(1–40) was dissolved in a 0.02% ammonia solution to 500 μM at 4 °C. Aβ-(1–40) amyloid fibrils were prepared by the fibril extension method as described previously (27). Seeds were prepared by the fragmentation of amyloid fibrils for 5 min with a TAITEC VP-30S sonicator (Saitama, Japan) equipped with a microtip. The seeds were added at a final concentration of 5 μg/ml to 50 μM monomeric Aβ-(1–40) in 50 mM sodium phosphate buffer at pH 7.5 and 100 mM NaCl. After 3 h at 37 °C in the test tube, 100 μM ThT was added at a final concentration of 5 μM. An aliquot (14 μl) of sample solution was deposited on each microscopic slide, and an image of the fibrils was obtained with TIRFM. The formation of Aβ-(1–40) fibrils on various

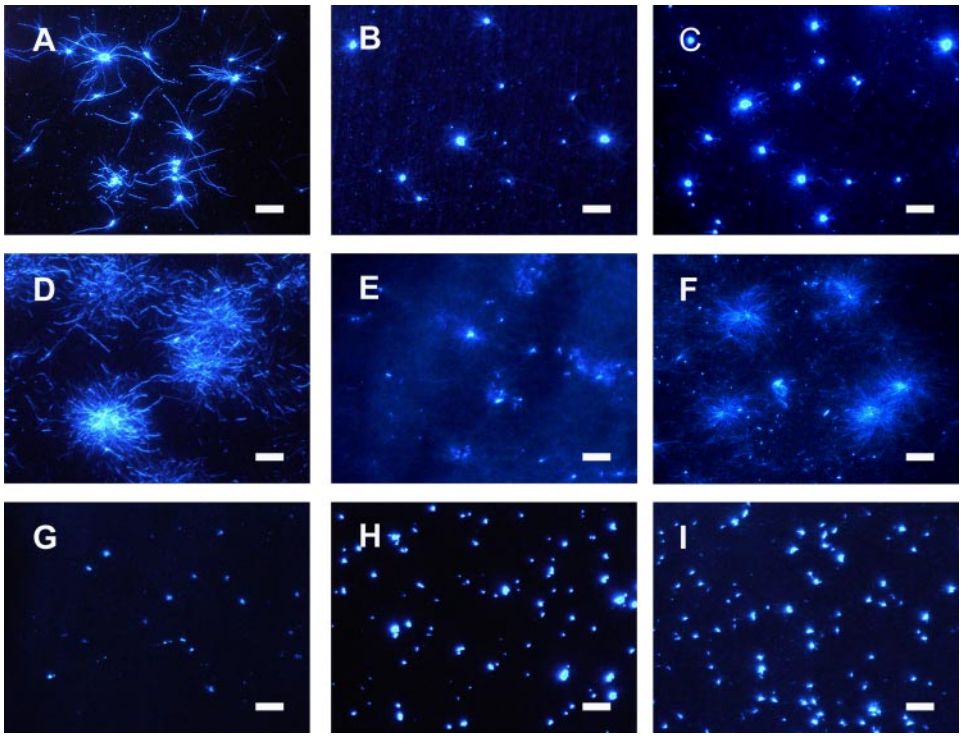

FIGURE 1. **Surface-dependent growth of Aβ-(1–40) amyloid fibrils.** Seed-dependent growth was performed on various surfaces: quartz (*A*), negatively charged 10-(carboxy)decyldimethylchlorosilane (*B*), negatively charged APTS/PVS (*C*), negatively charged PEI/PVS (*D*), negatively charged PEI/PSS (*E*), negatively charged PEI/PAA (*F*), hydrophobic OTS (*G*), positively charged APTS (*H*), and positively charged PEI (*I*). Concentrations of Aβ-(1–40) monomers, seeds, and ThT were 50 μM, 5 μg/ml, and 5 μM, respectively. The *scale bar* represents 10 μm. Extensive fibril growth was observed on the surfaces with negative charges *(panels A–F)*, whereas the formation of fibrils was suppressed on hydrophobic (*panel G*) or positively charged (*panels H* and *I*) surfaces.

TABLE 1
Physicochemical properties of the substrates and morphology of the Aβ fibrils

Surface materials	Surface charge	Water contact angle[a]	Fibril growth pattern
		°	
Quartz	Negative	0	Linear and radial
CDDS[b]	Negative	10	Linear and radial
PEI/PVS	Negative	0	Spherical
APTS/PVS	Negative	6	Spherical
PEI/PAA	Negative	24	Spherical
PEI/PSS	Negative	58	Spherical
OTS	Non-charged	105	No growth
APTS	Positive	62	No growth
PEI	Positive	35	No growth

[a] The water contact angle is the maximal angle between the surface of the substrate and that of the water droplet: Repulsion between the substrate and water makes the angle larger, thus giving a measure of the hydrophobicity of the substrate.
[b] 10-(carboxy)decyldimethylchlorosilane.

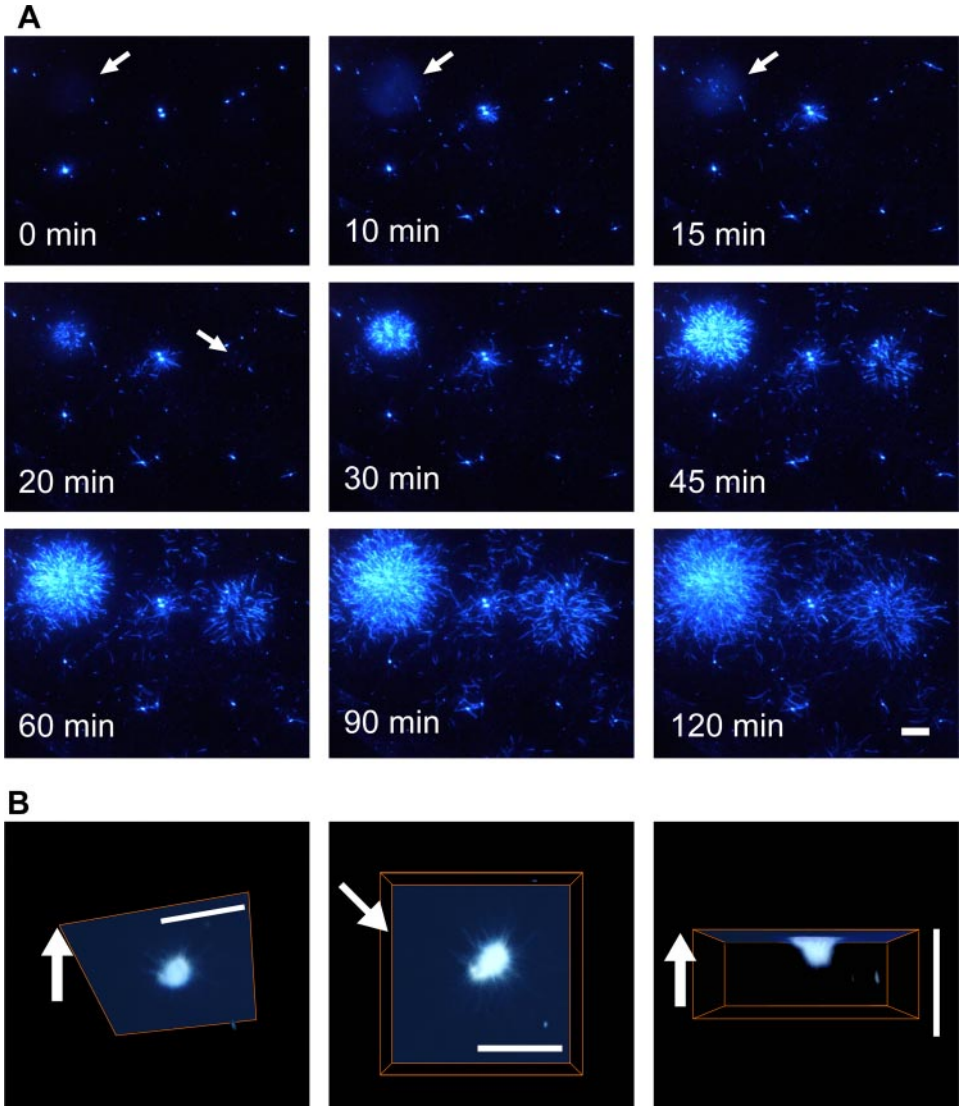

FIGURE 2. **Real-time observations of the formation of Aβ-(1–40) spherulitic structures.** *A*, real-time observations of Aβ-(1–40) amyloid fibril growth on PEI/PVS at pH 7.5 and 37 °C. Concentrations of Aβ-(1–40) monomers, seeds, and ThT were 50 μM, 5 μg/ml, and 5 μM, respectively. The *white arrows* in panels of 0–20 min indicate the hazy area detected before clear images of spherical amyloid fibrils were obtained. At time 0, large clusters were not observed on the surface. At 10 min, hazy globular objects were identified. At 15 min, fibrils emerged. Fibrils grew both in size and in number with time, forming huge spherical amyloid assemblies with a radius of more than 20 μm at 120 min. *B*, three-dimensional reconstruction of the spherical assembly on PEI/PVS observed by a laser scanning confocal microscopy. *Left*, overall view; *middle*, top view; and *right*, side view. The *arrows* indicate the direction of the upper side of the microscopic cell. This view focuses on the core regions, whereas peripheral regions with separated fibrils can be seen in the sectional images (Supplemental Movie 2). The *scale bars* in *panels A* and *B* represent 10 μm.

surfaces was also examined. After the mixing of the solutions of seeds, monomeric proteins, and ThT at the same final concentrations as above, the mixture was immediately deposited on the microscopic slide and incubated at 37 °C for 3 h.

For the real-time observation of Aβ-(1–40) amyloid fibril growth, the seed fibrils were added at a final concentration of 0.5 μg/ml to 50 μM monomeric Aβ-(1–40) in polymerization buffer (50 mM sodium phosphate buffer at pH 7.5 and 100 mM NaCl). The ThT solution was then added at a final concentration of 5 μM, sample mixtures were deposited on the PEI/PVS surface, and fibrils were observed every 2 min under TIRFM at 37 °C.

Laser Scanning Confocal Microscopy and Three-dimensional Reconstruction of Spherulitic Structures—For the confocal image observation, Aβ-(1–40) amyloid fibrils were prepared under the same conditions as used for the TIRFM observation. Confocal images were taken with a laser scanning confocal microscope (Fluoview FV1000, Olympus, Tokyo, Japan). ThT was excited by 458 nm light of a multi-argon laser. For through-focus imaging, all optical sections were collected with 0.25 μm *z* axis steps and were clarified through Kalman filtration. The three-dimensional reconstitution of stacked images was performed with Amira 4.0 (Mercury Computer Systems, Chelmsford, MA). Quartz crystal microbalance measurements are provided in Supplemental Fig. 3.

Transmission Electron Microscopy—The presence of amyloid fibrils in the spherulitic structures was examined by electron microscopy. After confirming the formation of spherulitic structures under TIRFM, the coverslip was carefully removed from the quartz substrate. An aliquot (5 μl) of distilled water was deposited on the substrate, and then carbon-coated copper grids (400 mesh) were put on the substrate for 3 min so as to transfer the fibrils. Then, the grids were stained with a 2% (w/v) uranyl acetate solution. Electron micrographs were acquired using a transmission microscope (100CX, JEOL, Tokyo, Japan) at 80 kV with magnification ×29,000.

RESULTS

Effects of Various Surfaces on the Formation of Aβ Fibrils—We observed the seed-dependent formation of Aβ-(1–40) fibrils on the surface of various chemically modified substrates that were created either by alternative adsorption of polyelectrolytes or with self-assembled monolayers of silanes. The results are compiled in Fig. 1 and Table 1. In the presence of the Aβ-(1–40) seed fibrils, enhanced fibril formation was observed on negatively charged surfaces, including quartz and PEI/PVS. On quartz, intense growth led to remarkably long fibrils as reported previously (Fig. 1*A*) (19). We often observed radial growth patterns suggesting the presence of clustered seeds. Real-time observation showed that once growth started, unidirectional growth continued until the depletion of monomers, producing long fibrils of uniform width (Supplemental Fig. 1). Such long fibrils were not observed in solution, indicating that moderate interaction with the surface prevents the lateral association of growing fibrils, thus enabling the persistent growth.

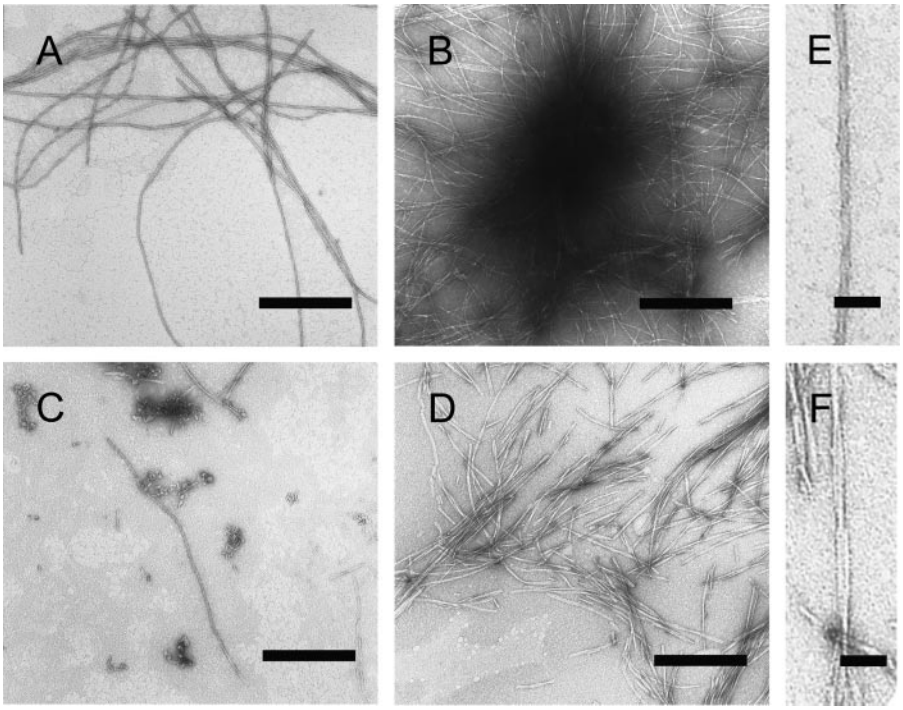

FIGURE 3. **Electron micrographs of the Aβ-(1–40) amyloid fibrils.** *A* and *B*, fibrils in the spherulitic structures formed on the PEI/PVS surface. The spherulitic structures were prepared on the PEI/PVS surface under the same conditions as used for the real-time observation. After confirmation of the spherulitic structures under TIRFM, they were transferred to a carbon grid and then analyzed by transmission electron microscopy with magnification ×29,000. *C*, fibrils formed on the quartz surface. *D*, fibrils formed in the test tube. Electron micrographs of fibrils on quartz surface were acquired by the same method as the fibrils on the PEI/PVS surface. *E* and *F*, enlarged images of fibrils taken from *panel A* (*E*) and *panel D* (*F*). The *scale bars* in *panels A–D* represent 400 nm, and those in *panels E* and *F* represent 50 nm.

Formation of Aβ Spherulitic Structures—Fibril growth was especially prominent on the surfaces covered with PEI/PVS, highly negatively charged and hydrophilic polyelectrolytes (Fig. 1*D*). We initially presumed that the growth of fibrils on the PEI/PVS initiated from large clustered seeds attached to the surface. However, the real-time observation revealed striking images of fibril growth, producing huge spherical assemblies with a densely packed radial pattern (Fig. 2*A* and Supplemental Movie 1). Importantly, no branching of the growing ends was observed as on quartz (see also Figs. 3 and 4, below).

We also examined the spherical assemblies by a laser scanning confocal microscopy; a three-dimensional reconstruction image (Fig. 2*B*) and all sectional images (Supplemental Movie 2) indicated that they are built up with ThT-positive amyloid fibrils. It is noted that the confocal microscopy image shown in Fig. 2*B* gives a close-up view of core regions.

To examine the presence of amyloid fibrils in the spherical assemblies, and moreover, their morphology at high resolution, we analyzed the spherical assemblies by transmission electron microscopy. After confirming the spherical assemblies under TIRFM, they were transferred from the PEI/PVS surface to a carbon grid and then analyzed by the electron microscopy with magnification ×29,000. Electron micrographs showed both separated fibrils (Fig. 3*A*) and clustered fibrils, suggesting a radial growth pattern (Fig. 3*B*). Expanded images revealed unbranched and twisted fibril morphology with a diameter of 7–14 nm, basically consistent with previous reports (Fig. 3*E*) (28). It is noted that transmission electron microscopy is not useful for reproducing the huge spherultic structures as reported for bovine insulin with a scanning electron microscopy (30). Moreover, the observed images suggest that the spherultic assemblies were partly broken during the transfer from PEI/PVS substrate to the carbon grids. However, we can fairly conclude that the spherical assemblies are made of typical amyloid fibrils. Similar fibrillar structures were also observed for the fibrils formed on a quartz surface, although their transfer to carbon-coated grids was less efficient (Fig. 3*C*). On the other hand, fibrils formed in the test tube exhibited more loosely coiled fibrils with a diameter of 15 nm (Fig. 3, *D* and *F*), suggesting that both quartz and PEI/PVS surfaces induced a slight morphological change. In particular, such a loosely coiled fibril was rarely observed in the spherical assemblies.

In the spherical assemblies, fibril growth continued linearly as on quartz, when length was plotted against time, until the depletion of monomers (Fig. 4). Incidentally, the rates of growth were similar (~0.3 μm/min) for both types of fibrils (19). This result supports morphological similarity of individual fibrils. Thus, once the fibril growth started, the rate of fibril growth might be less affected by the physicochemical properties of the surface, although the extents of seed clustering and adsorption significantly depend on the surface.

Considering that TIRFM illumination has a depth of penetration of ~150 nm and the depth of focus on the objective lens is about 100 nm, the large clusters of seeds formed at first *in solution* and were not in contact with the substrate. The hazy areas observed at the initial stages, as indicated in Fig. 2*A* by *arrows*, may represent the clustered seeds or aggregated intermediates formed in solution. Since the thickness of the water medium estimated from the fine focus stroke between the quartz slide and the coverslip is about 10 μm, the spherical assemblies observed here are in fact flattened spheres. However, three-dimensional reconstruction image based on confocal microscopy observation suggests that the core region is indeed spherical (Fig. 2*B*). The surface used for TIRFM observation was located on the upper side of the cell, so the clustered fibrils on the surface are not deposited by gravitational force.

As for other substrates, extensive fibril formation was generally observed on the surfaces with negative charges, regardless of whether they were modified by a polyelectrolyte or silane (Fig. 1, *A–F*). In contrast, fibril growth was largely suppressed on positively charged or hydrophobic surfaces (Fig. 1, *G–I*). The image obtained with hydrophobic surface suggested that the

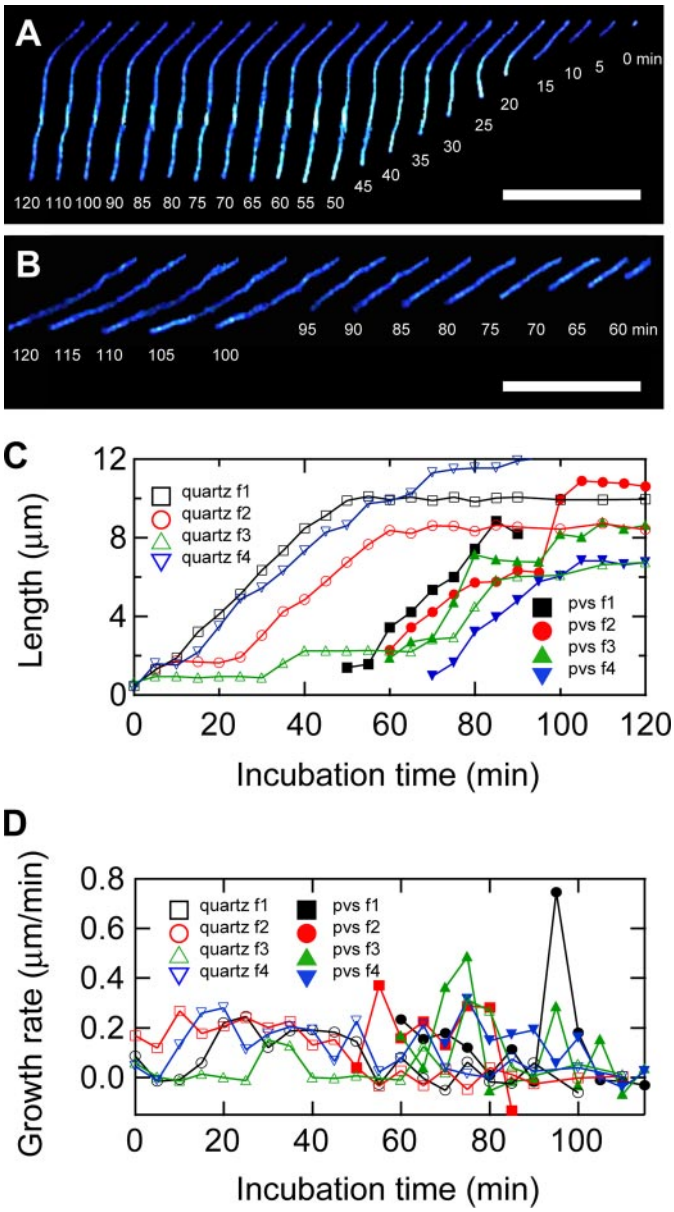

FIGURE 4. **Single fibrillar analysis of Aβ-(1–40) fibril growth.** *A* and *B*, direct observation of Aβ-(1–40) fibril growth on quartz (*A*) and in spherulitic assemblies (*B*) by TIRFM. *C*, fibril length was plotted against incubation time for various fibrils to obtain the growth rate (*D*). The fibrils used for the analysis were taken from Supplemental Fig. 1 for fibrils on quartz (*open symbols*) and from Fig. 2*A* for spherulitic fibrils (*solid symbols*). The *scale bars* in *panels A* and *B* represent 10 μm. Although the pause of fibril growth on quartz (*e.g. quartz f3*) is a real pause, the apparent pause and subsequent rapid growth of fibrils in spherulitic structures (*e.g. pvs f2*) would be caused by the transient disappearance of the fibrils from evanescent fields.

binding efficiency of seed fibrils are less than that of other surfaces. Thus, the efficiency of seed adsorption may be an important factor determining the fibril growth (see below). To examine the effects of seeding, we studied the spontaneous fibril formation with variously modified surfaces. Although a similar massive growth of fibrils was observed even for spontaneous fibril formation on the negatively charged surfaces, spontaneous fibril formation was also suppressed on the positively charged surfaces (Supplemental Fig. 2). We then confirmed that the observed morphological differences were induced during the fibril growth on the surface; loading of the fibrils pre-

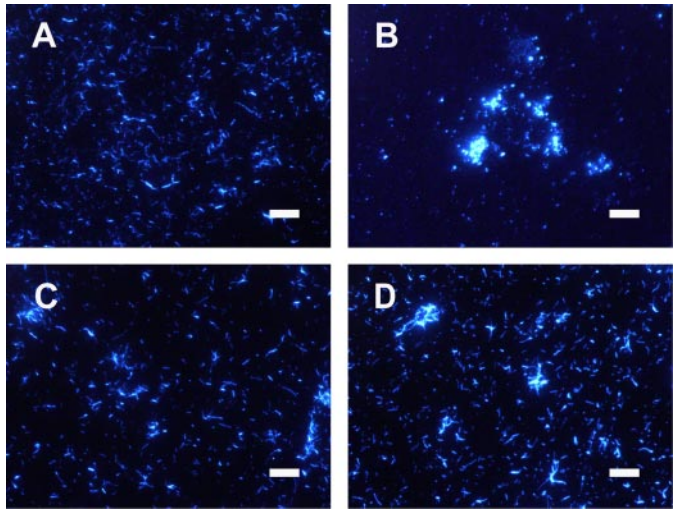

FIGURE 5. **TIRFM images of Aβ-(1–40) amyloid fibrils preformed in test tubes and loaded on various surfaces.** *A–D*, quartz (*A*), a hydrophobic OTS surface (*B*), a positively charged PEI surface (*C*), and a negatively charged PEI/PVS surface (*D*). Concentrations of Aβ-(1–40) monomers, seeds, and thioflavin T were 50 μM, 5 μg/ml, and 5 μM, respectively. The *scale bar* represents 10 μm. The relatively short and straight nature of the adsorbed fibrils was basically the same regardless of the properties of the surface, although fibril aggregates were observed on the hydrophobic surface (*B*), confirming that the observed morphological differences as shown in Fig. 1 were induced during the growth of fibrils on the surface.

formed in a test tube to various substrates did not induce the morphological changes (Fig. 5).

Interaction of Aβ with Various Surfaces—The Aβ-(1–40) sequence is divided into the polar region (1D-28K), with both positive (5R, 13H, 14H, 16K, 28K) and negative (1D, 3E, 7D, 11E, 22E, 23D) charges, and the hydrophobic transmembrane regions (29G-40V) (4). The net charge of Aβ-(1–40) at pH 7 is slightly negative. To address the interaction of Aβ with various surfaces, we used quartz crystal microbalance with dissipation monitoring, by which the mass and viscoelastic properties of bound ligands can be estimated (29). The results indicated that although Aβ monomers and fibrils bind to a variety of surfaces at pH 7, the binding of seed fibrils to the hydrophobic surface is less than that of others (Supplemental Fig. 3), consistent with the TIRFM observation (Fig. 1*G*). Importantly, the bound fibrils are more flexible on the negatively charged surface, probably because of the charge repulsion.

DISCUSSION

Formation of Senile Plaque-like Aβ Spherulitic Structures—Most importantly, the assemblies of Aβ-(1–40) fibrils observed in the present study resemble the amyloid core of senile plaques observed in the cerebral cortices of patients suffering from Alzheimer disease (5). Similar spherical amyloid deposits are observed in a mouse model of Alzheimer disease (16), in patients with Creutzfeldt-Jakob disease (17), and in several other neurodegenerative diseases (7). Furthermore, spherulites were observed *in vitro* in many systems including natural and synthetic polymers (see Ref. 30 for detail), for example in insulin (30, 31), pathogenic immunoglobulin chains (32), β-lactoglobulin (33), and synthetic peptides (34), indicating that they are a common architectural feature of fibers. We consider that the senile plaque-like spherical objects observed here correspond

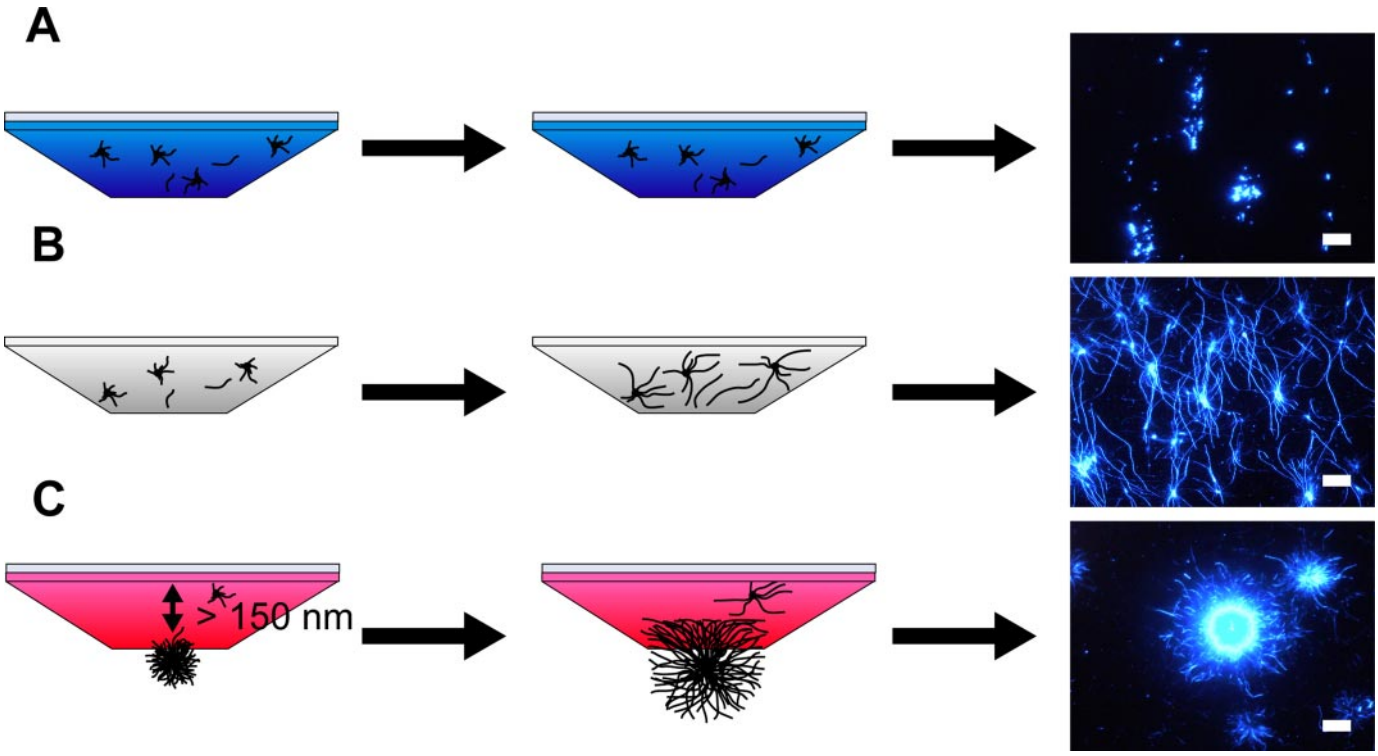

FIGURE 6. **Schematic representation of the surface-dependent fibril growth of Aβ-(1–40).** *A–C*, a positively charged surface (*A*), negatively charged quartz (*B*), and a negatively charged PEI/PVS multilayer surface (*C*). The *scale bars* in the *right column* represent 10 μm. Since the thickness of the water medium estimated from the fine focus stroke between the quartz slide and coverslip is about 10 μm, the spherulitic structures observed here are in fact flattened spheres.

to spherulites, a higher order spherical assembly of amyloid fibrils ranging in diameter from 10 to 150 μm. In a polarizing light microscope, spherulites exhibit a typical "Maltese-cross" extinction pattern (30). In the present study, we did not examine the presence of Maltese-cross since we could not isolate the spherical objects to perform the measurements under cross-polarizers. Thus, additional studies are necessary to conclude that the observed amyloid assemblies are indeed spherulites.

However, the similarity of the amyloid core of senile plaques and the spherulitic assemblies observed in the present study suggest that senile plaques in patients also develop through the cooperative growth and association of amyloid fibrils as visualized here, together with interactions between Aβ monomers/fibrils and various biological molecules. During concurrent fibril growth from clumped seeds, moderate repulsion between the fibrils may keep the growing ends separated and thus active. At the same time, moderate attraction between growing fibrils is presumably important to maintain the spherical shape. Thus, the formation of senile plaques is likely to be governed both by the physicochemical properties of Aβ amyloid fibrils *per se* and by the molecular environment *in situ*.

Effects of Surface on the Fibril Formation—Our observations with TIRFM are consistent with various reports studying the effects of surface on fibril formation. *In situ* atomic force microscopy of the amyloidogenic immunoglobulin light chain variable domain SMA showed that negatively charged SMA formed fibrils on the negatively charged mica surface, whereas fibrils did not form on the positively charged or hydrophobic surfaces (15). It has been reported that the formation of Aβ fibrils was facilitated by the negatively charged acidic phospholipids rather than neutral phospholipids (11). These reports also proposed that the strong electrostatic attractions tightly trap the seed fibrils on the surface so that the subsequent growth is inhibited. The inhibitory role of hydrophobic surface might be explained in a similar manner. Moreover, the slightly low efficiency of binding of amyloid precursors in the forms of monomers or seed fibrils to the hydrophobic surfaces might contribute to the suppressed fibril formation. Taken together, the effects of surface on the formation of Aβ-(1–40) fibrils can be classified into three types (Fig. 6).

First, tight electrostatic attraction between negatively charged Aβ-(1–40) and a positively charged surface is unfavorable for efficient fibril growth (Fig. 6*A*). Tight hydrophobic interaction is also unfavorable. Tight interactions may mask the growing ends. Flexibility of the growing ends might also be required for fibril growth. Moreover, adsorption to the surface decreases the concentration of active monomers, thus inhibiting the growth.

Second, even when the surface charge is moderately negative as in the case of quartz, Aβ-(1–40) with a net negative charge can bind to the surface through local electrostatic attraction and hydrophobic interaction. However, since the interaction is weaker, Aβ-(1–40) seeds expose their growing edge, ensuring efficient fibril growth (Fig. 6*B*). Weak binding of Aβ-(1–40) fibrils to quartz was evidenced by the transient disappearance of fibrils from evanescent fields monitored by TIRFM (19).

Third and most interestingly, PEI/PVS with a strongly negative and hydrophilic surface produced a huge spherical object, a spherulitic structure (Fig. 6*C*). The real-time observation showed that the main body of fibril growth indeed takes place

some distance from the surface (beyond the depth of penetration of the evanescent field) (Fig. 2). Thus, although overall observations point to a clear influence of solid surfaces on the formation of spherulitic structures, it remains unknown whether direct interactions with the surface are essential. One possibility is that increasing the local concentration of seed fibrils on the PEI/PVS surface, as revealed by the quartz crystal microbalance measurements, leads to the clustering of seeds. Then, the clustered seeds may detach from the surface, promoting the formation of spherulitic structures in solution. A similar effect has been suggested in the spontaneous formation of spherical aggregates of Aβ termed "β-amyl balls" (35). Once fibril growth started from the clustered seeds, the combination of intense growth and the delicate balance of repulsions and attractions enables the massive growth of fibrils in a radial pattern, producing a huge and harmonic object. Finally, we consider that the above models on the basis of the results with Aβ-(1–40) will be applicable to Aβ-(1–42), which is suggested to be the main component of senile amyloid plaques.

Conclusion—The surface properties have crucial roles in both promoting and suppressing the fibril growth and interactions. By controlling the surface properties, we reproduced the senile-plaque-like spherulitic assemblies of Aβ-(1–40). The real-time images at the single fibrillar level revealed that a balance of attractive and repulsive interactions coupled with intense growth without branching produces a huge spherical object. On the other hand, on a quartz surface, intense growth led to remarkably long fibrils, implying similarity to the deposition on vascular basement membranes. These observations argue that the physicochemical properties of amyloid fibrils *per se* play a dominant role for the formation of senile plaques, as well as deposition on vascular basement membranes, giving insights into creating the strategies for preventing Alzheimer disease.

Acknowledgments—We thank Dr. Tetsuichi Wazawa (Tohoku University) for support with the TIRFM system. Electron micrographs were taken using a facility in the Research Center For Ultrahigh Voltage Electron Microscopy, Osaka University.

REFERENCES

1. Dobson, C. M. (2003) *Nature* **426,** 884–890
2. Lansbury, P. T., Jr. (2004) *Nat. Med.* **10,** 13709–13715
3. Hardy, J., and Selkoe, D. (2002) *Science* **297,** 353–356
4. Mattson, M. P. (2004) *Nature* **430,** 631–639
5. Jin, L., Claborn, K., Kurimoto, M., Geday, M., Maezawa, I., Sohraby, F., Estrada, M., Kaminsky, W., and Kahr, B. (2003) *Proc. Natl. Acad. Sci. U. S. A.* **100,** 15294–15298
6. Naiki, H., and Nakakuki, K. (1996) *Lab. Investig.* **74,** 374–383
7. Harper, J. D., and Lansbury, P. T., Jr. (1997) *Annu. Rev. Biochem.* **66,** 385–407
8. McLaurin, J., Yang, D. S., Yip, C. M., and Fraser, P. E. (2000) *J. Struct. Biol.* **130,** 259–270
9. Petkova, A. T., Leapman, R. D., Guo, A., Yau, W. M., Mattson, M. P., and Tycko, R. (2005) *Science* **307,** 262–265
10. Kakio, A., Nishimoto, S., Yanagisawa, K., Kozutsumi, Y., and Matsuzaki, K. (2002) *Biochemistry* **41,** 7385–7390
11. Gellermann, G. P., Appel, T. R., Tannert, A., Radestock, A., Hortschansky, P., Schroeckh, V., Leisner, C., Lütkepohl, T., Shtrasburg, S., Röcken, C., Pras, M., Linke, R., Diekmann, S., and Fändrich, M. (2005) *Proc. Natl. Acad. Sci. U. S. A.* **102,** 6297–6302
12. Yip, C. M., Darabie, A. A., and Mclaurin, J. (2002) *J. Mol. Biol.* **318,** 97–107
13. Blackley, H. K. L., Sanders, G. H. W., Davies, M. C., Roberts, C. J., Tendler, S. J. B., and Wilkinson, M. J. (2000) *J. Mol. Biol.* **298,** 833–840
14. Kowalewski, T., and Holtzman, D. M. (1999) *Proc. Natl. Acad. Sci. U. S. A.* **96,** 3688–3693
15. Zhu, M., Souillac, P. O., Ionescu-Zanetti, C., Carter, S. A., and Fink, A. L. (2002) *J. Biol. Chem.* **277,** 50914–50922
16. Hsiao, K., Chapman, P., Nilsen, S., Eckman, C., Harigawa, Y., Younkin, S., and Yang, F., Cole, G. (1996) *Science* **274,** 99–102
17. Manuelidis, L., Fritch, W., and Xi, Y.-G. (1997) *Science* **277,** 94–98
18. Ban, T., Hamada, D., Hasegawa, K., Naiki, H., and Goto, Y. (2003) *J. Biol. Chem.* **278,** 16462–16465
19. Ban, T., Hoshino, M., Takahashi, S., Hamada, D., Hasegawa, K., Naiki, H., and Goto, Y. (2004) *J. Mol. Biol.* **344,** 757–767
20. Naiki, H., Higuchi, K., Hosokawa, M., and Takeda, T. (1989) *Anal. Biochem.* **177,** 244–249
21. Morigaki, K., and Walde, P. G. (2002) *Langmuir* **18,** 10509–10511
22. Xia, Y., Mrksich, M., Kim, E., and Whitesides, G. M. (1995) *J. Am. Chem. Soc.* **117,** 9576–9577
23. Jonas, U., del Campo, A., Kruger, C., Glasser, G., and Boos, D. (2002) *Proc. Natl. Acad. Sci. U. S. A.* **99,** 5034–5039
24. Anzai, J., Kobayashi, Y., Nakamura, N., Nishimura, M., and Hoshi, T. (1999) *Langmuir* **15,** 221–226
25. Decher, G. (1997) *Science* **277,** 1232–1237
26. Wazawa, T., and Ueda, M. (2005) *Adv. Biochem. Engin. Biotechonol.* **95,** 77–106
27. Hasegawa, K., Yamaguchi, I., Omata, S., Gejyo, F., and Naiki, H. (1999) *Biochemistry* **38,** 15514–15521
28. Goldsbury, C. S., Wirtz, S., Müller, S. A., Sunderji, S., Wicki, P., Aebi, U., and Frey, P. (2000) *J. Struct. Biol.* **130,** 217–231
29. Richter, R. P., and Brisson, A. R. (2005) *Biophys. J.* **88,** 3422–3433
30. Krebs, M. R. H., MacPhee, C. E., Miller, A. F., Dunlop, I. E., Dobson, C. M., and Donald, A. M. (2004) *Proc. Natl. Acad. Sci. U. S. A.* **101,** 14420–14424
31. Rogers, S. S., Krebs, M. R. H., Bromley, E. H. C., van der Linden, E., and Donald, A. M. (2006) *Biophys. J.* **90,** 1043–1054
32. Raffen, R., Dieckman, L. J., Szpunar, M., Wunschl, C., Pokkuluri, P., Dave, P., Stevens, P. W., Cai, X., Schiffer, M., and Stevens, F. J. (1999) *Protein Sci.* **8,** 509–517
33. Sagis, L. M. C., Veerman, C., and van der Linden, E. (2004) *Langmuir* **20,** 924–927
34. Fezoui, Y., Martley, D. M., Walsh, D. M., Selkoe, D. J., Osterhout, J. J., and Teplow, D. B. A. (2000) *Nat. Struct. Biol.* **7,** 1095–1099
35. Westlind-Danielsson, A., and Arnerup, G. (2001) *Biochemistry* **40,** 14736–14743

Real-time and Single Fibril Observation of the Formation of Amyloid β Spherulitic Structures

Tadato Ban, Kenichi Morigaki, Hisashi Yagi, Takashi Kawasaki, Atsuko Kobayashi, Shunsuke Yuba, Hironobu Naiki and Yuji Goto

J. Biol. Chem. 2006, 281:33677-33683.
doi: 10.1074/jbc.M606072200 originally published online September 7, 2006

Supplemental Data

Real-time and Single Fibril Observation of the Formation of Amyloid β Spherulitic Structures

Tadato Ban, Kenichi Morigaki, Hisashi, Yagi, Takashi Kawasaki, Atsuko Kobayashi, Syunsuke Yuba, Hironobu Naiki, and Yuji Goto

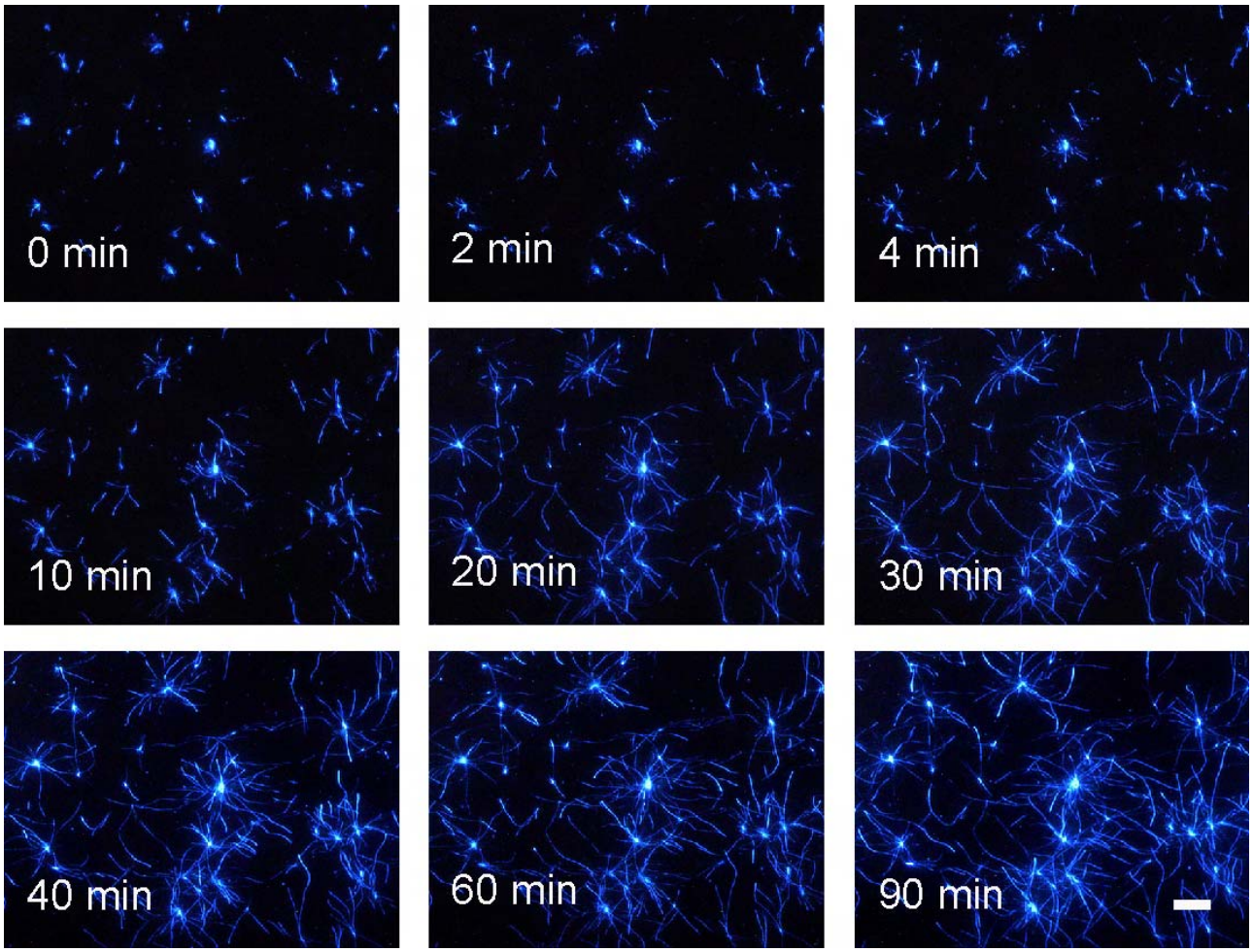

SUPPLEMENTAL FIGURE 1. Real-time monitoring of fibril growth on quartz surfaces. The scale bar represents 10 μm. A similar image and its movie file measured under the same conditions but of different experiment were published previously (1).

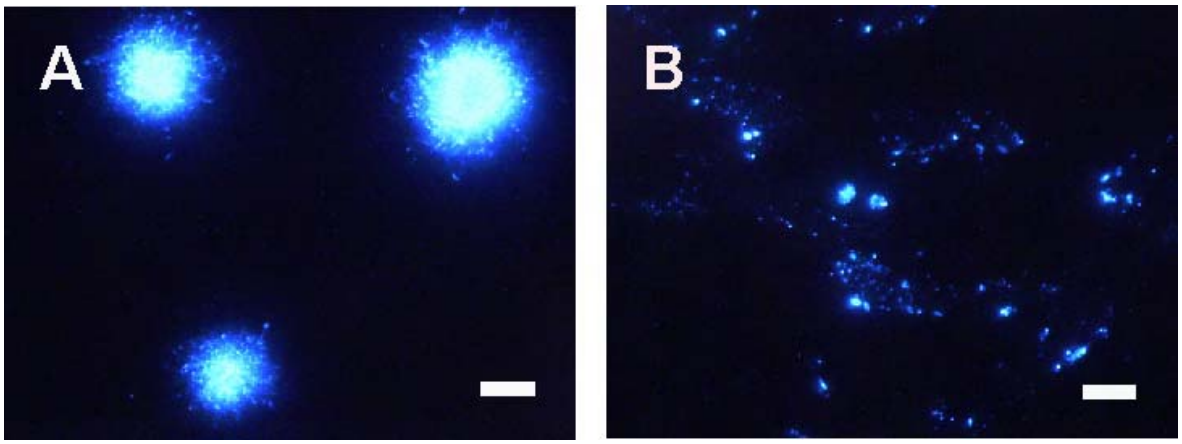

SUPPLEMENTAL FIGURE 2. TIRFM images of Aβ(1-40) amyloid fibrils formed spontaneously without seeds. (A) On the negatively charged PVS surface and (B) positively charged PEI surface. The scale bars represent 10 μm.

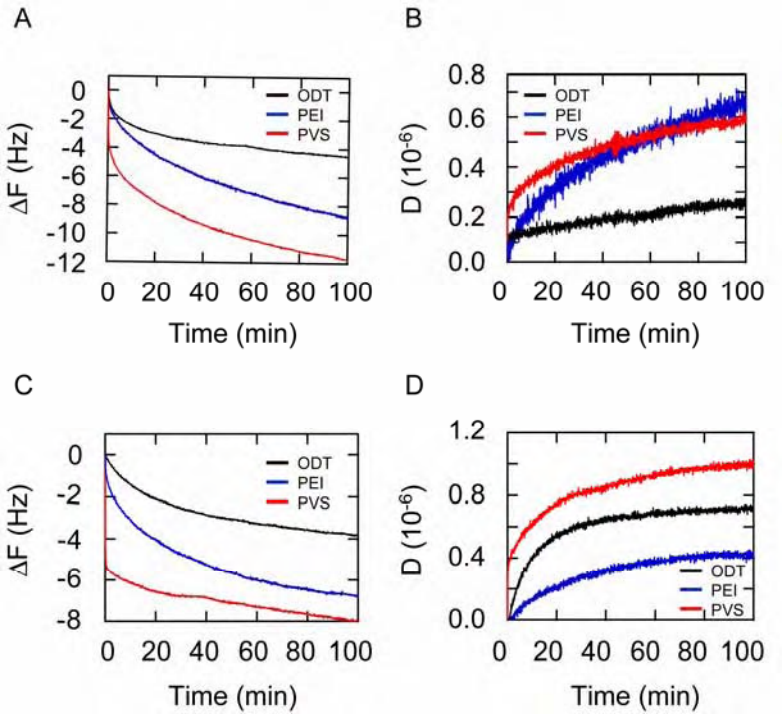

SUPPLEMENTAL FIGURE 3. QCM-D analysis of the interaction of Aβ(1-40) with various surfaces. QCM response changes in frequency and dissipation on ODT, PEI and PVS surfaces (a, b) for the adsorption of monomeric Aβ(1-40) and (c, d) for the adsorption of Aβ(1-40) seed fibrils. Concentrations of Aβ(1-40) monomers and seed fibrils were 7.5 μM and 5 μg/ml, respectively. For both Aβ monomers and fibrils, the charged surfaces exhibited stronger binding than the hydrophobic surface. The change of dissipation upon binding indicated that the bound monomers are more flexible on the charged surfaces than on the hydrophobic surface. The flexibility of the bound monomers was similar between the positively charged and negatively charged surfaces, but greater than on the hydrophobic surface. On the other hand, the flexibility of the bound fibrils varied in the order: negatively charged surface > hydrophobic surface > positively charged surface. QCM-D measurements were performed with the Q-Sense D300 system with a QAFC 302 axial flow chamber (Göteborg, Sweden) (2). The QCM sensor crystal was oscillated at its resonance frequency of 5 MHz and the frequency shift (*f*) and dissipation (*D*) were monitored at three harmonics (15, 25, and 35 MHz). The interval for data acquisition was 0.4 s. Chemically modified QCM sensor surfaces were prepared using self-assembled monolayers of 1-ocatadecanthiol, 2-aminoethanethiol, or mercaptoacetic acid (Sigma-Aldrich, St. Louis., USA) to give hydrophobic, positively charged and negatively charged surfaces, respectively. The mounted QCM sensor crystal was equilibrated with a degassed buffer solution at 21.8 °C. The buffer solution was subsequently replaced with the sample solution. Concentrations of Aβ(1-40) monomer and seed fibrils were 7.5 μM and 18 .8 μg/ml, respectively.

SUPPLEMENTAL MOVIES

Supplemental Movie 1. Real-time monitoring of the growth of Aβ(1-40) fibrils on PEI/PVS monitored by TIRFM. pH 7.5 and 37 °C. Representative images are shown in Fig. 2A. The conditions are described in the legend of Fig. 2A.

Supplemental Movie 2. Sectional images of the spherical assembly of Aβ(1-40) fibrils on PEI/PVS monitored by laser scanning confocal microscopy. pH 7.5 and 37 °C. 3D reconstruction images are shown in Fig. 2B. All optical sections were collected with 0.25 μm z-axis steps and were clarified through Kalman filtration.

SUPPLEMENTAL REFERENCES

1. Ban, T., Hoshino, M., Takahashi, S., Hamada, D., Hasegawa, K., Naiki, H., and Goto, Y. (2004) *J. Mol. Biol*. **344**, 757-767.
2. Richter, R. P. Maury, N., and Brisson, A. R. (2005) *Langmuir* **21**, 299-304.